# Ultrafast Structural Dynamics along the $\beta - \gamma$ Phase Transition Path in MnAs

Franck Vidal,[1] Yunlin Zheng,[1] Lounès Lounis,[1,2] Leticia Coelho,[1,3] Claire Laulhé,[4,5] Carlo Spezzani,[6,7] Alessandra Ciavardini,[4] Horia Popescu,[4] Eugenio Ferrari,[7,8] Enrico Allaria,[7] Jialin Ma,[9] Hailong Wang,[9] Jianhua Zhao,[9] Matthieu Chollet,[10] Matthew Seaberg,[10] Roberto Alonso-Mori,[10] James M. Glownia,[10] Mahmoud Eddrief,[1] and Maurizio Sacchi[1,4]

[1]*Sorbonne Université, CNRS, Institut des NanoSciences de Paris, INSP, F-75005 Paris, France*

[2]*PSL Research University, 75231 Paris, France*

[3]*Instituto de Física, Universidade de Brasília UnB, Brasília - DF, CEP 70910-900, Brazil*

[4]*Synchrotron SOLEIL, L'Orme des Merisiers, Saint-Aubin BP 48, 91192 Gif-sur-Yvette Cedex, France*

[5]*Université Paris-Saclay (Université Paris-Sud), F-91405 Orsay Cedex, France*

[6]*Laboratoire de Physique des Solides, CNRS, Université Paris-Sud, Université Paris-Saclay, 91405 Orsay Cedex, France*

[7]*FERMI-ELETTRA Sincrotrone Trieste, in Area Science Park, S.S.14, Km 163.5, I-34149 Trieste, Italy*

[8]*Particle Accelerator Physics Laboratory, Ecole Polytechnique Fédérale de Lausanne, 1015 Lausanne, Switzerland*

[9]*State Key Laboratory of Superlattices and Microstructures, Institute of Semiconductors, Chinese Academy of Sciences, P. O. Box 912, Beijing 100083, P. R. China*

[10]*Linac Coherent Light Source (LCLS), SLAC National Accelerator Laboratory, Menlo Park, California 94025, USA*

## Abstract

We investigate the orthorhombic distortion and the structural dynamics of epitaxial MnAs layers on GaAs(001) using static and time-resolved x-ray diffraction. Laser-induced intensity oscillations of Bragg reflections allow us to identify the optical phonon associated with orthorhombic distortion and to follow its softening along the path towards an undistorted phase of hexagonal symmetry. The frequency of this mode falls in the THz range, in agreement with recent calculations. Incomplete softening suggests that the $\beta - \gamma$ transformation deviates from a purely second-order displacive transition.

MnAs is a semi-metal that has attracted considerable interest since its discovery in the early 1900s [1, 2]. Current ongoing research on MnAs is motivated by its applications as a magnetocaloric material [3, 4] or in spintronic devices [5–9]. Moreover, temperature- and laser-driven magnetization reversal have been achieved in an Fe layer deposited on the MnAs/GaAs(001) heteroepitaxial system [10, 11]. The potential of MnAs for applications derives from a peculiar sequence of magneto-structural phase transitions [12, 13], which have been studied at a fundamental level for decades but are not fully understood yet. In the bulk, at low temperatures, the most stable crystal structure is hexagonal (NiAs-type, space group $P6_3/mmc$, see Fig. 1a), and ferromagnetic (FM) order is observed. This phase is commonly noted as $\alpha$-MnAs. At $T_c$=313 K, a first-order phase transition occurs, FM order is lost and the structure becomes orthorhombic ($\beta$-MnAs, MnP-type, space group $Pnma$, see Fig. 1b). The orthorhombic distortion parameter $\eta$, equal to one at $T_c$, progressively vanishes through a second-order phase transition at $T_t \simeq 400$ K, where the hexagonal symmetry is recovered ($\gamma$-MnAs).

The mechanisms leading to this peculiar sequence have been studied extensively [14–18]. Recent density-functional theory (DFT) calculations suggest that the $\beta - \gamma$ transformation is a displacive phase transition driven by the softening of a THz mode located at the edge of the hexagonal Brillouin zone (BZ), with normal coordinate along $\eta$ [19, 20]. This soft mode would also be implied in the $\alpha - \beta$ transition because of strong spin-phonon coupling. Indirect signatures of – at least partial – phonon softening can be found in the literature [21, 22], supporting the hypothesis of a phonon mechanism for these phase transitions. However, no direct experimental measurements of phonons in MnAs have been reported to date. Considering the low frequency and the possible strong damping of the soft mode, its spectroscopic signature may be elusive in frequency-domain experiments.

In this letter, we investigate the laser-excited soft coherent phonons in MnAs, using femtosecond time-resolved x-ray diffraction. The temperature and fluence dependent intensity oscillations were measured for selected Bragg reflections that feature different responses to the orthorhombic distortion $\eta$. The latter parameter could be probed in a wide range of values, near ambient temperature, by using a strained MnAs/GaAs(001) thin film to perform our study.

A 70-nm thick MnAs epitaxial film was grown by molecular beam epitaxy on GaAs(001) [23]. The epitaxial relationship with $\vec{c} \parallel [001]_{\mathrm{GaAs}}$ and $\vec{a} \parallel [1\bar{1}0]_{\mathrm{GaAs}}$ was checked by labo-

ratory x-ray diffraction measurements. When MnAs is grown on GaAs(001), the epitaxial constraints have a strong impact on the sequence of phase transitions. In particular, the $\beta$-phase can be already stabilized at 278 K, *i.e.* 35 K below the bulk crystal $T_c$. As the temperature increases, the $\alpha$ and $\beta$ phases coexist up to 313 K, when the $\alpha$ phase disappears. Both the premature appearance of $\beta$ and the $\alpha - \beta$ phase coexistence in MnAs/GaAs(001) have been studied by various techniques [24–30]. However, no measurements of the orthorhombic distortion of $\beta$-MnAs in epitaxial thin films have been reported in the literature.

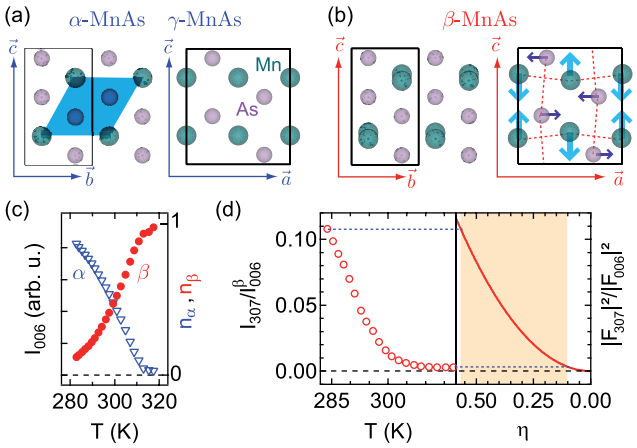



FIG. 1: (Color online) (a) $\alpha/\gamma$-MnAs hexagonal crystal structure. The orthorhombic system is used in order to describe each phase of MnAs with a common Bravais lattice. The shaded area indicates the hexagonal cell. (b) $\beta$-MnAs orthorhombic crystal structure. Arrows indicate the displacement along the $A_g$ mode coordinates, corresponding to a reduction of the orthorhombic distortion $\eta$. Dashed lines are a guide to the eye, highlighting the distortion. (c) Intensity of the $\alpha$ (triangles) and $\beta$ (disks) 006 Bragg reflections as a function of the temperature. (d) Left panel: ratio of the 307 and 006 Bragg reflection intensities for the $\beta$-phase in MnAs/GaAs(001) as a function of the temperature. Right panel: calculated ratio of the squared modulus of structure factors of the 307 and 006 Bragg reflections as a function of the orthorhombic distortion $\eta$. The shaded area indicates the $\eta$ range probed in our experiment. All Bragg reflections are indexed within the orthorhombic axes.

Prior to the time-resolved experiments, we determined the temperature dependence of the orthorhombic distortion of the $\beta$-MnAs phase within MnAs/GaAs(001) thin films, by means of x-ray diffraction measurements carried out at the CRISTAL beamline of SOLEIL

synchrotron, using 9.5 keV radiation. The sample temperature was controlled by a Peltier thermoelectric module and monitored by using a thermocouple. In the following, Bragg reflections are indexed within the orthorhombic axes for all MnAs phases. The diffracted intensity and the structure factor of a $hk\ell$ reflection will be labeled as $I_{hk\ell}$ and $F_{hk\ell}$, respectively. $I_{006}$ and $I_{307}$ were monitored as a function of the temperature over the 280 K-320 K range. The intensities of the $\alpha$ and $\beta$ 006 reflections, denoted $I^{\alpha}_{006}$ and $I^{\beta}_{006}$, allow us to retrieve the relative volume fractions of the two phases, $n_\alpha$ and $n_\beta$. The results are displayed in Fig.1(c). The 307 reflection is forbidden in the hexagonal symmetry and the squared modulus of its structure factor, $|F_{307}|^2$, is a monotonically increasing function of $\eta$. This reflection can thus be used to monitor the orthorhombic distortion in the system. As $n_\beta$ increases with the temperature, we use the $I_{307}/I^{\beta}_{006}$ ratio, independent of $n_\beta$, in order to monitor $\eta$. Fig.

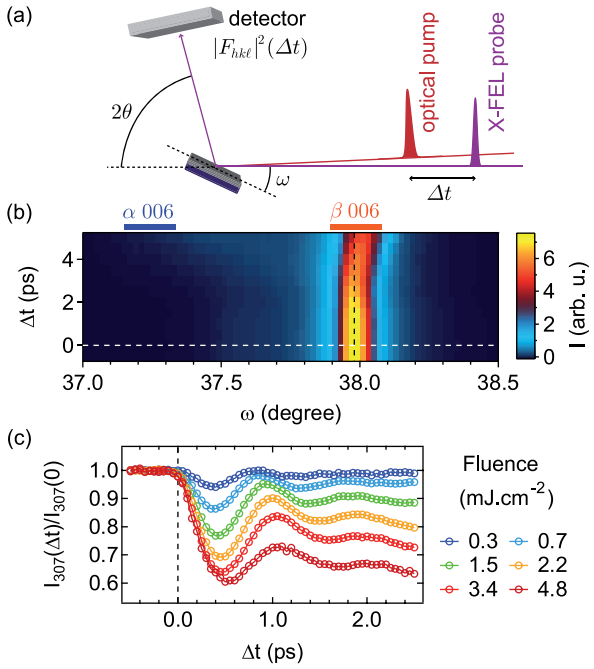



FIG. 2: (Color online) (a) Experimental setup used for time-resolved x-ray diffraction measurements. Scans were performed in the vertical bisecting mode, with $\omega$ the incidence angle of x-rays with respect to the sample surface, and $2\theta$ the detection angle. $\Delta t$ is the time delay between x-ray probe and optical pump. (b) Delay-angle map for the 006 reflection at $T$=320 K, $\Phi$=8 mJ/cm$^2$. (c) Time dependence of the normalized intensity of the 307 Bragg reflection at $T$=293 K for several pump fluences.

1(d) compares the measured ratio as a function of the temperature with the one calculated as a function of $\eta$, showing that, for our epitaxial layer, the [0.1-0.6] $\eta$ range can be probed around room temperature. This is at variance with bulk MnAs where $\eta$ drops gradually when approaching the $\beta \rightarrow \gamma$ phase transition at the higher temperature of 400 K [13]. At 318 K the volume of the orthorhombic cell is equal to 135.3 Å$^3$ in MnAs/GaAs(001), as deduced from lattice parameters values extracted from our diffraction measurements. This is larger than the bulk value of 134 Å$^3$ and closer to 136.5 Å$^3$, *i.e.* to the critical value for which the distortion disappears at $T_t$ in the bulk, as shown by diffraction [12, 31] and DFT calculations [18]. Therefore, the depressed distortion as compared to the bulk can be linked to the peculiar strain state of MnAs/GaAs(001), with $\beta$-MnAs in tension. Summarizing: (i) $\alpha$ and $\beta$ phases coexist in the 280-313 K range, (ii) $\eta$ decreases with temperature, from 0.6 to 0.1, and (iii) beyond 313 K, the system is in the pure $\beta$ phase with a lower value of $\eta$ than in the bulk. We note that epitaxial layers on GaAs(001) offer the possibility of stabilizing $\beta$-MnAs with a wide range of $\eta$ values over a narrow temperature range near ambient. This is beneficial to the investigation of THz phonons, since working at temperatures much lower than $T_t$ reduces the influence of phonon-phonon scattering on the damping of low frequency modes.

Time resolved x-ray diffraction measurements were performed at the XPP beamline of the Linac Coherent Light Source (LCLS) free electron laser in Stanford [32], using the experimental geometry depicted in Fig. 2(a). The sample was excited by a pump laser pulse (800 nm wavelength, 43 fs duration FWHM, penetration depth 20 nm) and probed by 9.5 keV x-ray pulses (35 fs duration FWHM) at a 120 Hz repetition rate. The arrival time of each pulse was monitored by using the timing tool available at XPP [33], providing an overall time resolution of 55 fs. Fig. 2(b) shows $I^{\beta}_{006}$ at $T$=320 K (pure $\beta$-phase) as a function of the incidence angle and of the pump-probe delay $\Delta t$. Up to $\Delta t$=2.5 ps, the angular position of the Bragg peak does not change. Beyond this delay, a shift is observed, a consequence of strain building following strain wave generation and propagation within the thin film [36]. In the following, we restrict our analysis of time-resolved experiments to the $\Delta t \leq 2.5$ ps range, where variations of the diffracted intensity are not related to the strain-induced peak shift.

The soft mode that is expected to participate in the $\gamma \rightarrow \beta$ transition has its counterpart at $\Gamma$ in the orthorhombic BZ. The associated atomic motions take place along the coordinate

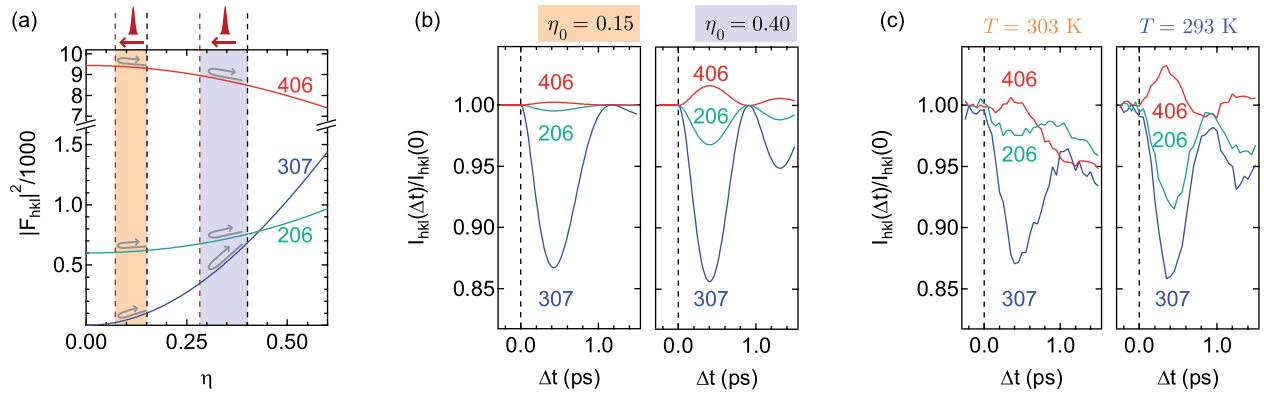



FIG. 3: (Color online) (a) Variation of $|F^{\beta}_{206}|^2$, $|F_{307}|^2$ and $|F^{\beta}_{406}|^2$ with the orthorhombic distortion $\eta$. The shaded areas represent qualitatively the $\eta$ intervals that are spanned after the laser pulse arrival at delay 0, with U-turn arrows symbolizing the coherent oscillations of $\eta$. (b) Simulated time dependence of $I^{\beta}_{206}$, $I_{307}$ and $I^{\beta}_{406}$ starting from $\eta_0$=0.15 and $\eta_0$=0.40 at negative delay. (c) Time dependence of the normalized diffracted intensity for the 206, 307, and 406 Bragg reflections measured at $T$=293 K ($\Phi$=0.7 mJ/cm$^2$) and $T$=303 K ($\Phi$=1.5 mJ/cm$^2$).

of the orthorhombic distortion $\eta$, as depicted schematically by arrows in Fig. 1(b). Such a mode, of $A_g$ symmetry, can be excited coherently through the displacive excitation mechanism [34, 35]. Since the density of states of $\beta$-MnAs is dominated by anti-bonding states above the Fermi level [37], electronic excitations will result in a more symmetric potential energy surface, allowing for displacive excitations. Fig. 2(c) shows the temporal evolution of $I_{307}$ for various pump fluences ($\Phi$). The data show oscillations at approximately 1 THz, a frequency that matches the one predicted in Ref. 20. The laser-induced dynamics changes upon increase of the pump fluence: the frequency of the oscillations decreases, damping increases and the diffracted intensity at $\Delta t \geq 2$ ps drops. This trend is particularly marked for fluences above 2 mJ/cm$^2$ and can be ascribed to increasing disorder and to the subsequent appearance of a strong Debye-Waller term in the dynamical response. In the following we restrict our analysis to fluences below 2 mJ/cm$^2$.

In order to check whether the oscillating diffracted intensity originates from variations of the amplitude of the orthorhombic distortion, we measured the dynamics of several $hk\ell$ reflections: the 107 and 307 reflections forbidden in the hexagonal phase, and the 206 and 406 reflections, allowed for both hexagonal and orthorhombic symmetries but featuring

opposite variations of the intensity as a function of $\eta$. We make use of the very distinct dependence on $\eta$ of the structure factors of these reflections, Fig. 3(a), to prove that the atomic displacements associated with the observed oscillations of Bragg peak intensities are consistent with a variation of $\eta$. Indeed, the slopes of the $|F_{hk\ell}|^2(\eta)$ curves determine the sign and amplitude of the coherent oscillations. Assuming a coherent excitation of the mode with normal coordinates along $\eta$, $F_{hk\ell}(\Delta t)$ can be derived using the following expressions:

$$F_{hk\ell}(\Delta t) = F_{hk\ell}(\eta_0 - \Delta\eta) \tag{1}$$

$$\Delta\eta = \Delta\eta_0(e^{-\Delta t/\tau_{disp}} - \cos(2\pi\nu\Delta t)e^{-\Delta t/\tau_{osc}}) \tag{2}$$

where $\eta_0$ is the static value of the distortion, $\nu$ is the optical mode frequency, $\tau_{disp}$ is the relaxation time of the displacive excitation and $\tau_{osc}$ is the damping time constant of the vibration. $\Delta\eta$ is the coherently driven modulation of the distortion with amplitude $\Delta\eta_0$. Fig. 3(b) shows simulations of $I_{hk\ell}(\Delta t)$ for 406, 206 and 307 reflections, using eqs. 1-2 and taking into account the finite pump penetration depth. Since at low fluence excitation $\tau_{osc}$ and $\tau_{disp}$ are of the same order of magnitude [see Fig. 2(c) for 0.3 mJ/cm$^2$], we used a single time constant $\tau$. Curves in Fig. 3(b) are obtained with $\eta_0$=0.15, $\Delta\eta_0$=0.15, $\nu$=0.8 THz, $\tau$=0.4 ps, and with $\eta_0$=0.40, $\Delta\eta_0$=0.20, $\nu$=1.1 THz, $\tau$=0.8 ps. Starting from $\eta_0$=0.40, we have $\partial|F_{206}|^2/\partial\eta > 0$ and $\partial|F_{307}|^2/\partial\eta > 0$, resulting in an initial reduction of the diffracted intensity, while $\partial|F_{406}|^2/\partial\eta < 0$ results in an initial increase of the signal, as shown in Fig. 3(b). When $\eta_0$ decreases, $|F_{206}|^2(\eta)$ and $|F_{406}|^2(\eta)$ flatten and coherent oscillations of the associated Bragg peaks are expected to vanish, as shown in Fig. 3(b) for $\eta_0$=0.15.

Fig. 3(c) shows the time dependence of the normalized diffracted intensity for the 206, 307, and 406 Bragg reflections at $T$=293 K and $T$=303 K, which correspond to high and low values of $\eta_0$, respectively. The agreement with simulated data is good, with the most salient features well reproduced: the sign and the amplitude of the oscillations correspond to the calculations displayed in Fig. 3 (b). Results obtained at $T$=293 K and $T$=303 K match well the oscillations of $\eta$ starting from $\eta_0$=0.40 and $\eta_0$= 0.15, respectively. These $\eta_0$ values are consistent with those determined from the static, temperature-dependent measurements presented in Fig. 1(d). Experimental data and simulations match also for 006 and 107 reflections, which have the same $\eta$-dependence as 406 and 307, respectively. This good agreement allows us to ascribe the observed oscillations to the coherent excitation of an optical mode with atomic displacements having the symmetry required to drive the $\beta - \gamma$

phase transition.

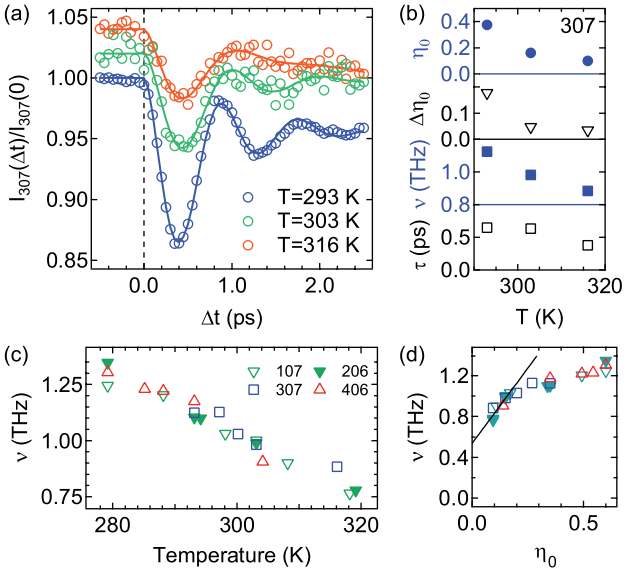



FIG. 4: (Color online) (a) Normalized $I_{307}$ vs. delay ($\Phi$=0.7 mJ/cm$^2$) at three different temperatures (symbols) and corresponding fits (lines) obtained using Eq. (3). Data are shifted vertically for clarity. (b) Fitted parameters associated with data in (a). (c) Frequency $\nu$ of $\beta$-MnAs zone-center optical phonon as a function of the temperature, obtained by fitting the time-dependent intensities of 107, 206, 307 and 406 reflections ($\Phi$=0.7 mJ/cm$^2$). (d) Same values as in (c) plotted against $\eta_0$. The straight line fits $\nu(\eta_0)$ values for $\eta_0 < 0.2$, pointing at $\nu(0)$=0.53 THz.

We now discuss the variation of $\nu$ with temperature, the parameter we use to control $\eta_0$ (see Fig. 1). In the limit of purely second order displacive phase transitions, the frequency of the soft-mode is expected to be directly proportional to the order parameter, and should tend to 0 as the critical temperature is approached [38]. In the $\gamma$ phase, the frequency of the predicted soft-mode involved in the $\gamma \rightarrow \beta$ transition is expected to cancel at the transition temperature. Its parent mode in the $\beta$-phase, the zone-center optical mode probed in the present study, should also soften when approaching the transition. In order to extract $\nu$ from the time-resolved measurements, oscillations of the normalized diffraction intensity were fitted with the following *ad hoc* function:

$$\frac{I(\Delta t)}{I_0} = \frac{|F_{hk\ell}(\Delta t)|^2}{|F_{hk\ell}(\eta_0)|^2}[1 - \Delta I(1 - e^{-\Delta t/\tau_1})] \qquad (3)$$

In this expression, $\Delta I$ and $\tau_1$ describe the fact that the diffracted intensity does not recover in the short delays range due to increasing disorder. $\eta_0$ was fixed to the value determined by

static diffraction measurements. An example of fitted time dependence is displayed in Fig. 4(a) for the 307 reflection, with fit parameters in Fig. 4(b). $\Delta I$ and $\tau_1$ were found to be of the order of few percents and few ps, respectively. Focusing on the parameter describing the phonon oscillation, $\Delta\eta_0$ decreases with the temperature as a result of the decrease in efficiency of the displacive mechanism as $\eta \to 0$ and $\tau$ also decreases as a consequence of stronger anharmonic effects. A significant decrease of $\nu$ is observed, which is confirmed by the analysis of the time dependence of $I_{107}$, $I_{206}$, $I_{307}$, and $I_{406}$ in the temperature range under investigation. The fitted values of $\nu$ at low pump fluence are given in Fig. 4(c). The measured frequencies fall in a range compatible with the calculated frequency, $\nu$=0.943 THz, for bulk MnAs [20] and $\nu$ decreases as the temperature increases: we have $\nu\simeq$1.3 THz at 278 K ($\eta_0$=0.6) and $\nu\simeq$0.8 THz at 320 K ($\eta_0$=0.1). We thus have a strong decrease of $\nu$ when $\eta_0 \to 0$, as shown in Fig. 4(d), yet the extrapolation towards $\eta_0$=0 suggests incomplete softening of the mode with $\nu$=0.53$\pm$0.07 THz. We note that correcting the measured frequency to account for the effect of the damping can only reduce the drop at low $\eta_0$ values.

The fact that $\nu$ does not vanish could be due to the stress field in $\beta$-MnAs/GaAs(001). However, this can be ruled out by quantifying the order of magnitude of the frequency change induced by stress. From Ref. 20, which gives the dependence of $\nu$ with pressure $P$, the maximum value of $|\partial\nu/\partial P|$ is $\sim$0.4 THz/GPa. Stress values in $\beta$-MnAs/GaAs(001) at 318 K are smaller than 0.1 GPa [39], leading to an estimated frequency shift smaller than 0.04 THz. Thus, our results indicate that the $\beta - \gamma$ transition is not of purely displacive second-order character with a single order parameter. Incomplete softening may be indicative of a certain order-disorder degree of the transition [40–42] or of the fact that other order parameters may be involved [43], leading to a distinct evolution of the phonon frequency [44]. In this respect, evidencing – or excluding – the predicted short-ranged antiferromagnetic order [20] of $\beta$-MnAs remains a challenge to be addressed before further time-resolved studies can disentangle the complex interplay of electronic and structural degrees of freedom [45, 46].

In conclusion, a predicted THz optical phonon mode, implied in the $\beta - \gamma$ transition of MnAs, has been evidenced. The obtained results provide a firm basis of comparison for future theoretical work on MnAs. From a more general perspective, we note that the use of epitaxial systems offers some advantages for the investigation of phase transitions. Notably, the ability to stabilize a given phase at temperatures lower than in the bulk can be favorable

in the analysis of anharmonic, strongly damped, soft modes by time-resolved techniques.

We acknowledge SOLEIL for provision of synchrotron radiation facilities. Use of the Linac Coherent Light Source (LCLS), SLAC National Accelerator Laboratory, is supported by the U.S. Department of Energy, Office of Science, Office of Basic Energy Sciences under Contract No. DE-AC02-76SF00515. We acknowledge support from CNRS through the PEPS-SASLELX program. E. Ferrari acknowledges the support of the Swiss National Science Foundation under grant IZK0Z2-175481. We also acknowledge the support from the National Natural Science Foundation of China under Grant No. U1632264.

---

[1] F. Heusler, Z. Angew. Chem. **17**, 260 (1904).

[2] S. Hilpert and T. Dieckmann, Ber. Dtsch. Chem. Ges. A **44**, 2378 (1911).

[3] D. H. Mosca, F. Vidal, and V. H. Etgens, Phys. Rev. Lett. **101**, 125503 (2008).

[4] J.-Y. Duquesne, J.-Y. Prieur, J. A. Canalejo, V. H. Etgens, M. Eddrief, A. L. Ferreira, and M. Marangolo, Phys. Rev. B **86**, 035207 (2012).

[5] S. Sugahara and M. Tanaka, Appl. Phys. Lett. **80**, 1969 (2002).

[6] M. Ramsteiner, H. Y. Hao, A. Kawaharazuka, H. J. Zhu, M. Kastner, R. Hey, L. Däweritz, H. T. Grahn, and K. H. Ploog, Phys. Rev. B **66**, 081304(R) (2002).

[7] V. Garcia, H. Jaffrès, J.-M. George, M. Marangolo, M. Eddrief, and V. H. Etgens, Phys. Rev. Lett. **97**, 246802 (2006).

[8] P. N. Hai, S. Ohya, M. Tanaka, S. E.Barnes, and S. Maekawa, Nature **458**, 489 (2009).

[9] M. E. Nowakowski, G. D. Fuchs, S. Mack, N. Samarth, and D. D. Awschalom, Phys. Rev. Lett. **105**, 137206 (2010).

[10] C. Spezzani, F. Vidal, R. Delaunay, M. Eddrief, M. Marangolo, V. Etgens, H. Popescu, and M. Sacchi, Sci. Rep. **5**, 8120 (2015).

[11] C. Spezzani, E. Ferrari, E. Allaria, F. Vidal, A. Ciavardini, R. Delaunay, F. Capotondi, E. Pedersoli, M. Coreno, C. Svetina, *et al.*, Phys. Rev. Lett. **113**, 247202 (2014).

[12] B. T. M. Willis and H. P. Rooksby, Proc. Phys. Soc. B **67**, 290 (1954).

[13] H. Wilson and J. S. Kasper, Acta Crystallogr. **17**, 95 (1964).

[14] C. Kittel, Phys. Rev. **120**, 335 (1960).

[15] C. P. Bean and D. S. Rodbell, Phys. Rev. **126**, 104 (1962).

[16] N. Menyuk, J. A. Kafalas, K. Dwight, and J. B. Goodenough, Phys. Rev. **177**, 942 (1969).

[17] L. Pytlik and A. Zieba, J. Magn. Magn.Mater. **51**, 199 (1985).

[18] I. Rungger and S. Sanvito, Phys. Rev. B **74**, 024429 (2006).

[19] J. Łażewski, P. Piekarz, J. Toboła, B. Wiendlocha, P. T. Jochym, M. Sternik, and K. Parlinski, Phys. Rev. Lett. **104**, 147205 (2010).

[20] J. Łażewski, P. Piekarz, and K. Parlinski, Phys. Rev. B **83**, 054108 (2011).

[21] K. Bärner and H. Berg, Phys. Stat. Sol. (a) **49**, 545 (1978).

[22] J. D. Zou, H. Wada, B. G. Shen, J. R. Sun, and W. Li, Europhys. Lett. **81**, 47002 (2008).

[23] L. Lounis, M. Eddrief, M. Sacchi, and F. Vidal, Appl. Phys. Lett. **111**, 232403 (2017).

[24] L. Däweritz, Rep. Prog. Phys. **69**, 2581 (2006).

[25] V. M. Kaganer, B. Jenichen, F. Schippan, W. Braun, L. Däweritz, and K. H. Ploog Phys. Rev. B **66**, 045305 (2002).

[26] R. Magalhães-Paniago, L. N. Coelho, B. R. A. Neves, H. Westfahl, F. Iikawa, L. Däweritz, C. Spezzani, M. Sacchi, Appl. Phys. Lett. **86**, 053112 (2005).

[27] C. Adriano, C. Giles, O. D. D. Couto, M. J. S. P. Brasil, F. Iikawa, L. Däweritz, Appl. Phys. Lett. **88**, 151906 (2006).

[28] F. Vidal, O. Pluchery, N. Witkowski, V. Garcia, M. Marangolo, V. H. Etgens, Y. Borensztein, Phys. Rev. B **74**, 115330 (2006).

[29] R. Breitwieser, F. Vidal, I. L. Graff, M. Marangolo, M. Eddrief, J.-C. Boulliard, and V. H. Etgens, Phys. Rev. B **80**, 045403 (2009).

[30] C. Mocuta, D. Bonamy, S. Stanescu, S. El Moussaoui, A. Barbier, F. Montaigne, F. Maccherozzi, E. Bauer, and R. Belkhou, Sci. Rep. **7**, 16970 (2017).

[31] T. Suzuki and H. Ido, J. Phys. Soc. Jpn. **51**, 3149 (1982).

[32] M. Chollet, R. Alonso-Mori, M. Cammarata, D. Damiani, J. Defever, J. T. Delor, Y. Feng, J. M. Glownia, J. B. Langton, S. Nelson, *et al.*, J. Synchrotron Radiat. **22**, 503 (2015).

[33] M. Harmand, R. Coffee, M. R. Bionta, M. Chollet, D. French, D. Zhu, D. M. Fritz, H. T. Lemke, N. Medvedev, B. Ziaja, S. Toleikis, and M. Cammarata, Nature Photon. **7**, 215 (2013).

[34] H. J. Zeiger, J. Vidal, T. K. Cheng, E. P. Ippen, G. Dresselhaus, and M. S. Dresselhaus, Phys. Rev. B **45**, 768 (1992).

[35] S. L. Johnson, M. Savoini, P. Beaud, G. Ingold, U. Staub, F. Carbone, L. Castiglioni, M. Hengsberger, and J. Osterwalder, Struct. Dyn. **4**, 061506 (2017).

[36] C. Rose-Petruck, R. Jimenez, T. Guo, A. Cavalleri, C. W. Siders, F. Ráksi, J. A. Squier, B. C. Walker, K. R. Wilson, and C. P. J. Barty, Nature **398**, 310 (1999).

[37] C. Paduani, Solid State Commun. **150**, 2294 (2010).

[38] J. F. Scott, Rev. Mod. Phys. **46**, 83 (1974).

[39] A. K. Das, C. Pampuch, A. Ney, T. Hesjedal, L. Däweritz, R. Koch, and K. H. Ploog, Phys. Rev. Lett. **91**, 087203 (2003).

[40] A. D. Bruce, K. A. Müller, and W. Berlinger, Phys. Rev. Lett. **42**, 185 (1979).

[41] J. Hlinka, T. Ostapchuk, D. Nuzhnyy, J. Petzelt, P. Kuzel, C. Kadlec, P. Vanek, I. Ponomareva, and L. Bellaiche, Phys. Rev. Lett. **101**, 167402 (2008).

[42] T. Kohmoto, M. Masui, M. Abe, T. Moriyasu, and K. Tanaka, Phys. Rev. B **83**, 064304 (2011).

[43] J. W. Harter, D. M. Kennes, H. Chu, A. de la Torre, Z. Y. Zhao, J.-Q. Yan, D. G. Mandrus, A. J. Millis, and D. Hsieh, Phys. Rev. Lett. **120**, 047601 (2018).

[44] H. Schäfer, V.V. Kabanov, M. Beyer, K. Biljakovic, and J. Demsar, Phys. Rev. Lett. **105**, 066402 (2010).

[45] P. Beaud, A. Caviezel, S. O. Mariager, L. Rettig, G. Ingold, C. Dornes, S-W. Huang, J. A. Johnson, M. Radovic, T. Huber, T. Kubacka, A. Ferrer, H. T. Lemke, M. Chollet, D. Zhu, J. M. Glownia, M. Sikorski, A. Robert, H.Wadati, M. Nakamura, M. Kawasaki, Y. Tokura, S. L. Johnson, and U. Staub, Nat. Mater. **13**, 923 (2014).

[46] S. O. Mariager, C. Dornes, J. A. Johnson, A. Ferrer, S. Grübel, T. Huber, A. Caviezel, S. L. Johnson, T. Eichhorn, G. Jakob, H. J. Elmers, P. Beaud, C. Quitmann, and G. Ingold, Phys. Rev. B **90**, 161103(R) (2014).